Research Article | Vol. 6, No. 8 | 1 Aug 2016 | OPTICAL MATERIALS EXPRESS 2475

Optical Materials EXPRESS

Direct generation of dip-type sidebands from WS_2 mode-locked fiber laser

BO GUO,[1,4] QUAN LYU,[2] YONG YAO,[2] AND PENGFEI WANG[1,3,5]

[1]*Key Lab of In-Fiber Integrated Optics of Ministry of Education, Harbin Engineering University, Harbin 150001,China*
[2]*School of Electronic and Information Engineering, Shenzhen Graduate School, Harbin Institute of Technology, Shenzhen, 518055, China*
[3]*Photonics Research Centre, Dublin Institute of Technology, Kevin Street, Dublin 8, Ireland*
[4]*guobo512@163.com*
[5]*pengfei.wang@dit.ie*

Abstract: In this paper, we demonstrated the direct generation of dip-type sidebands from a passively mode-locked fiber laser based on the evanescent field interaction of two-dimensional material WS_2 and microfiber. The WS_2 nanosheets in polyvinyl alcohol solution are prepared through the liquid-phase exfoliation method and transferred onto a tapered fiber by the optical deposition method. The WS_2-deposited microfiber device could both operate as a mode-locker for soliton generation and induce a strong polarization effect to constitute an artificial polarizer for dip-type sidebands formation. In experiment, six kinds of dip-sidebands, namely, dip-dip type, hybrid peak-dip and dip type (I, II), dual-peak-dip type (I, II), and nearly-flat-top type are achieved by properly adjusting the pump strength and the polarization state in the laser cavity. Study found that the dynamic evolution of the dip-type sidebands along with the pump power is not reversible. In addition, we also obtained the maximum depth of ~16.8 dB and ~22 dB for dual-peak-dip type I and dual-peak-dip type II, respectively, and their second-order forms. Our study shows clearly that WS_2-assisted microfiber device can be as a mode-locker for soliton generation and a polarizer for studying nonlinear optics phenomenon in the fiber lasers simultaneously.

OCIS codes: (140.3510) Lasers, fiber; (140.4050) Mode-locked lasers; (160.4330) Nonlinear optical materials; (250.5530) Pulse propagation and temporal solitons.

References and links

1. U. Keller, "Recent developments in compact ultrafast lasers," Nature **424**(6950), 831–838 (2003).
2. M. E. Ferman and I. Hartl, "Ultrafast fibre lasers," Nat. Photonics **7**(11), 868–874 (2013).
3. I. N. Iii, "All-fiber ring soliton laser mode locked with a nonlinear mirror," Opt. Lett. **16**(8), 539–541 (1991).
4. K. Tamura, E. P. Ippen, H. A. Haus, and L. E. Nelson, "77-fs pulse generation from a stretched-pulse mode-locked all-fiber ring laser," Opt. Lett. **18**(13), 1080–1082 (1993).
5. O. G. Okhotnikov, T. Jouhti, J. Konttinen, S. Karirinne, and M. Pessa, "1.5-μm monolithic GaInNAs semiconductor saturable-absorber mode locking of an erbium fiber laser," Opt. Lett. **28**(5), 364–366 (2003).
6. Q. Bao, H. Zhang, Y. Wang, Z. Ni, Y. Yan, Z. X. Shen, K. P. Loh, and D. Y. Tang, "Atomic-layer graphene as a saturable absorber for ultrafast pulsed lasers," Adv. Funct. Mater. **19**(19), 3077–3083 (2009).
7. A. Martinez and Z. Sun, "Nanotube and graphene saturable absorbers for fibre lasers," Nat. Photonics **7**(11), 842–845 (2013).
8. C. Zhao, H. Zhang, X. Qi, Y. Chen, Z. Wang, S. Wen, and D. Tang, "Ultra-short pulse generation by a topological insulator based saturable absorber," Appl. Phys. Lett. **101**(21), 211106 (2012).
9. B. Guo, Y. Yao, Y.-F. Yang, Y.-J. Yuan, L. Jin, B. Yan, and J.-Y. Zhang, "Dual-wavelength rectangular pulse erbium-doped fiber laser based on topological insulator saturable absorber," Photon. Res. **3**, 94–99 (2015).
10. B. Guo, Y. Yao, J. Xiao, R. L. Wang, and J. Y. Zhang, "Topological insulator-assisted dual-wavelength fiber laser delivering versatile pulse patterns," IEEE J. Sel. Top. Quantum Electron. **22**(2), 1–8 (2016).
11. Y. Chen, G. Jiang, S. Chen, Z. Guo, X. Yu, C. Zhao, H. Zhang, Q. Bao, S. Wen, D. Tang, and D. Fan, "Mechanically exfoliated black phosphorus as a new saturable absorber for both Q-switching and Mode-locking laser operation," Opt. Express **23**(10), 12823–12833 (2015).
12. S. M. J. Kelly, "Characteristic sideband instability of periodically amplified average soliton," Elec. Lett. **28**(8), 806–807 (1992).
13. N. J. Smith, K. J. Blow, and I. Andonovic, "Sideband generation through perturbations to the average soliton model," J. Lightwave Technol. **10**(10), 1329–1333 (1992).
14. D. U. Noske, N. Pandit, and J. R. Taylor, "Source of spectral and temporal instability in soliton fiber lasers," Opt. Lett. **17**(21), 1515–1517 (1992).

#263278 http://dx.doi.org/10.1364/OME.6.002475
Journal © 2016 Received 15 Apr 2016; revised 5 Jun 2016; accepted 16 Jun 2016; published 7 Jul 2016

Optical Materials EXPRESS

15. M. L. Dennis and I. N. Duling III, "Experimental study of sideband generation in femtosecond fiber lasers," IEEE J. Quantum Electron. **30**(6), 1469–1477 (1994).
16. F. Matera, A. Mecozzi, M. Romagnoli, and M. Settembre, "Sideband instability induced by periodic power variation in long-distance fiber links," Opt. Lett. **18**(18), 1499–1501 (1993).
17. L. M. Zhao, D. Y. Tang, X. Wu, H. Zhang, C. Lu, and H. Y. Tam, "Observation of dip-type sidebands in a soliton fiber laser," Opt. Commun. **283**(2), 340–343 (2010).
18. J. N. Coleman, M. Lotya, A. O'Neill, S. D. Bergin, P. J. King, U. Khan, K. Young, A. Gaucher, S. De, R. J. Smith, I. V. Shvets, S. K. Arora, G. Stanton, H. Y. Kim, K. Lee, G. T. Kim, G. S. Duesberg, T. Hallam, J. J. Boland, J. J. Wang, J. F. Donegan, J. C. Grunlan, G. Moriarty, A. Shmeliov, R. J. Nicholls, J. M. Perkins, E. M. Grieveson, K. Theuwissen, D. W. McComb, P. D. Nellist, and V. Nicolosi, "Two-dimensional nanosheets produced by liquid exfoliation of layered materials," Science **331**(6017), 568–571 (2011).
19. Q. H. Wang, K. Kalantar-Zadeh, A. Kis, J. N. Coleman, and M. S. Strano, "Electronics and optoelectronics of two-dimensional transition metal dichalcogenides," Nat. Nanotechnol. **7**(11), 699–712 (2012).
20. M. Chhowalla, H. S. Shin, G. Eda, L. J. Li, K. P. Loh, and H. Zhang, "The chemistry of two-dimensional layered transition metal dichalcogenide nanosheets," Nat. Chem. **5**(4), 263–275 (2013).
21. F. Xia, H. Wang, D. Xiao, M. Dubey, and A. Ramasubramaniam, "Two-dimensional material nanophotonics," Nat. Photonics **8**(12), 899–907 (2014).
22. K. Wang, J. Wang, J. Fan, M. Lotya, A. O'Neill, D. Fox, Y. Feng, X. Zhang, B. Jiang, Q. Zhao, H. Zhang, J. N. Coleman, L. Zhang, and W. J. Blau, "Ultrafast saturable absorption of two-dimensional MoS_2 nanosheets," ACS Nano **7**(10), 9260–9267 (2013).
23. H. Zhang, S. B. Lu, J. Zheng, J. Du, S. C. Wen, D. Y. Tang, and K. P. Loh, "Molybdenum disulfide (MoS_2) as a broadband saturable absorber for ultra-fast photonics," Opt. Express **22**(6), 7249–7260 (2014).
24. H. Xia, H. Li, C. Lan, C. Li, X. Zhang, S. Zhang, and Y. Liu, "Ultrafast erbium-doped fiber laser mode-locked by a CVD-grown molybdenum disulfide (MoS_2) saturable absorber," Opt. Express **22**(14), 17341–17348 (2014).
25. H. Liu, A. P. Luo, F. Z. Wang, R. Tang, M. Liu, Z. C. Luo, W. C. Xu, C. J. Zhao, and H. Zhang, "Femtosecond pulse erbium-doped fiber laser by a few-layer MoS_2 saturable absorber," Opt. Lett. **39**(15), 4591–4594 (2014).
26. D. Mao, Y. Wang, C. Ma, L. Han, B. Jiang, X. Gan, S. Hua, W. Zhang, T. Mei, and J. Zhao, "WS_2 mode-locked ultrafast fiber laser," Sci. Rep. **5**, 7965 (2015).
27. P. Yan, A. Liu, Y. Chen, H. Chen, S. Ruan, C. Guo, S. Chen, L. Li, H. Yang, J. Hu, and G. Cao, "Microfiber-based WS_2-film saturable absorber for ultra-fast photonics," Opt. Mater. Express **5**(3), 479–489 (2015).
28. K. Wu, X. Zhang, J. Wang, and J. Chen, "463-MHz fundamental mode-locked fiber laser based on few-layer $MoS_{(2)}$ saturable absorber," Opt. Lett. **40**(7), 1374–1377 (2015).
29. M. Jung, J. Lee, J. Park, J. Koo, Y. M. Jhon, and J. H. Lee, "Mode-locked, 1.94-μm, all-fiberized laser using WS_2 based evanescent field interaction," Opt. Express **23**(15), 19996–20006 (2015).
30. R. Khazaeinezhad, S. H. Kassani, H. Jeong, K. J. Park, B. Y. Kim, D. I. Yeom, and K. Oh, "Ultrafast pulsed all-fiber laser based on tapered fiber enclosed by few-layer WS_2 nano-sheets," IEEE Photonics Technol. Lett. **27**(15), 1581–1584 (2015).
31. Z. Luo, D. Wu, B. Xu, H. Xu, Z. Cai, J. Peng, J. Weng, S. Xu, C. Zhu, F. Wang, Z. Sun, H. Zhang, and H. Zhang, "Two-dimensional material-based saturable absorbers: towards compact visible-wavelength all-fiber pulsed lasers," Nanoscale **8**(2), 1066–1072 (2016).
32. D. Mao, B. Du, D. Yang, S. Zhang, Y. Wang, W. Zhang, X. She, H. Cheng, H. Zeng, and J. Zhao, "Nonlinear Saturable Absorption of Liquid-Exfoliated Molybdenum/Tungsten Ditelluride Nanosheets," Small **12**(11), 1489–1497 (2016).
33. Z. Luo, Y. Huang, M. Zhong, Y. Li, J. Wu, B. Xu, H. Xu, Z. Cai, J. Peng, and J. Weng, "1-, 1.5-, and 2-μm fiber lasers Q-switched by a broadband few-layer MoS_2 saturable absorber," J. Lightwave Technol. **32**(24), 4077–4084 (2014).
34. R. I. Woodward, E. J. R. Kelleher, R. C. T. Howe, G. Hu, F. Torrisi, T. Hasan, S. V. Popov, and J. R. Taylor, "Tunable Q-switched fiber laser based on saturable edge-state absorption in few-layer molybdenum disulfide (MoS_2)," Opt. Express **22**(25), 31113–31122 (2014).
35. S. H. Kassani, R. Khazaeizhad, H. Jeong, T. Nazari, D. I. Yeom, and K. Oh, "All-fiber Er-doped Q-Switched laser based on Tungsten Disulfide saturable absorber," Opt. Mater. Express **5**(2), 373–379 (2015).
36. J. H. Chen, G. Q. Deng, S. C. Yan, C. Li, K. Xi, F. Xu, and Y. Q. Lu, "Microfiber-coupler-assisted control of wavelength tuning for Q-switched fiber laser with few-layer molybdenum disulfide nanoplates," Opt. Lett. **40**(15), 3576–3579 (2015).
37. B. Chen, X. Zhang, K. Wu, H. Wang, J. Wang, and J. Chen, "Q-switched fiber laser based on transition metal dichalcogenides MoS_2, $MoSe_2$, WS_2, and WSe_2," Opt. Express **23**(20), 26723–26737 (2015).
38. J. Ren, S. Wang, Z. Cheng, H. Yu, H. Zhang, Y. Chen, L. Mei, and P. Wang, "Passively Q-switched nanosecond erbium-doped fiber laser with MoS_2 saturable absorber," Opt. Express **23**(5), 5607–5613 (2015).
39. B. Guo, Y. Yao, P. G. Yan, K. Xu, J. J. Liu, S. G. Wang, and Y. Li, "Dual-wavelength soliton mode-locked fiber laser with a WS_2-based fiber taper," IEEE Photonics Technol. Lett. **28**(3), 323–326 (2016).
40. G. P. Agrawal, *Nonlinear Fiber Optics,* 5th ed. (Academic, 2013).
41. H. Zhang, D. Y. Tang, L. M. Zhao, and N. Xiang, "Coherent energy exchange between components of a vector soliton in fiber lasers," Opt. Express **16**(17), 12618–12623 (2008).
42. J. H. Wong, K. Wu, H. H. Liu, C. Ouyang, H. Wang, S. Aditya, P. Shum, S. Fu, E. J. R. Kelleher, A. Chernov, and E. D. Obraztsova, "Vector solitons in a laser passively mode-locked by single-wall carbon nanotubes," Opt. Commun. **284**(7), 2007–2011 (2011).
43. Y. F. Song, L. Li, H. Zhang, Y. Shen, D. Y. Tang, and K. P. Loh, "Vector multi-soliton operation and interaction in a graphene mode-locked fiber laser," Opt. Express **21**(8), 10010–10018 (2013).

Optical Materials EXPRESS

44. Q. Y. Ning, H. Liu, X. W. Zheng, W. Yu, A. P. Luo, X. G. Huang, Z. C. Luo, W. C. Xu, S. H. Xu, and Z. M. Yang, "Vector nature of multi-soliton patterns in a passively mode-locked figure-eight fiber laser," Opt. Express **22**(10), 11900–11911 (2014).
45. D. Goldstein, *Polarized Light*, 2nd ed. (Marcel Dekker, 2003).
46. R. A. Bergh, H. C. Lefevre, and H. J. Shaw, "Single-mode fiber-optic polarizer," Opt. Lett. **5**(11), 479–481 (1980).
47. G. Y. Li and A. S. Xu, "Analysis of the TE-pass or TM-pass metal-clad polarizer with a resonant buffer layer," J. Lightwave Technol. **26**(10), 1234–1241 (2008).
48. Q. Bao, H. Zhang, B. Wang, Z. Ni, C. H. Y. X. Lim, Y. Wang, D. Y. Tang, and K. P. Loh, "Broadband graphene polarizer," Nat. Photonics **5**(7), 411–415 (2011).
49. Z. Q. Luo, J. Z. Wang, M. Zhou, H. Y. Xu, Z. P. Cai, and C. C. Ye, "Multiwavelength mode-locked erbium-doped fiber laser based on the interaction of graphene and fiber-taper evanescent field," Laser Phys. Lett. **9**(3), 229–233 (2012).

1. Introduction

Over the past few decades, mode-locked fiber lasers have gained great attentions owing to their important applications in versatile fields such as nonlinear optics, laser spectroscopy, condensed matter physics, and material micromachining [1, 2]. So far, many passive mode-locking methods, including the nonlinear amplifying loop mirror (NALM) [3], nonlinear polarization rotation (NPR) [4], semiconductor saturable absorber mirror (SESAM) [5], graphene [6], carbon nanotubes (CNTs) [7], topological insulators (TIs) [8–10], and black phosphorus [11], have been used to obtain the soliton pulse in the fiber lasers. It is well-known that a typical characteristic of the soliton mode-locked lasers is the appearance of a series of discrete sidebands on their optical spectra. In 1992, Kelly firstly observed these spectral sidebands in a fiber laser and found that they follow an inverse square root dependence on the amplification period [12]. Thus, we call them Kelly sidebands. Thereafter, the nature and evolution mechanism of Kelly sidebands in the mode-locked lasers have been fully explored [13–15].

Interestingly, apart from the Kelly sidebands, Matera *et al.* also proposed a dip-type sideband generation on light propagating in an optic link with periodic power variation [16]. They pointed out that the even orders of dip-type sidebands have nearly the same frequency locations as those of the Kelly sidebands within the experimental parameter range of soliton fiber lasers. Thus, it makes the experimental identification of dip-type sideband becomes very difficult. Followed by this work, Zhao *et al.* reported the experimental observation of dip-type sidebands on the soliton spectra of a passively mode-locked fiber laser based on the NPR [17]. They attributed the formation of dip-type sidebands to a parametric process between the soliton and dispersive waves, which caused by the strong periodic soliton energy variation in the laser cavity. Different from the Kelly sidebands, the generation of dip-type sidebands is a threshold effect and their appearance will effect on the stability of fiber laser. Then, a series of questions arised naturally: is the generation of dip-type sidebands an intrinsic feature of the mode-locked lasers? Besides the NPR mechanism, whether other mode-locked scheme can be used to obtain the dip-type sidebands or not? How many patterns of dip-type sidebands exist? And do they have high-order form like Kelly sidebands? Clearly, the exploration of these questions about the generation and evolution mechanism of dip-type sidebands will help us to understand the nature of mode-locked lasers and design the new type of ultrafast fiber laser.

Recently, a novel kind of layered nanomaterial: transition metal dichalcogenides (TMDs), has attracted huge interesting in the fields of material, physics, chemistry and biology due to its potential applications in optoelectronic and biological industry [18–21]. In 2013, Wang *et al.* firstly revealed that MoS_2 nanosheet exhibits significant saturable absorption behavior [22]. Since then, TMDs including MoS_2, $MoSe_2$, $MoTe_2$, WS_2, WSe_2, and WTe_2 have been used for mode-locked [23–32] or Q-switched [33–38] fiber lasers at the wavelength range of 0.6-2 μm owing to their broadband saturable absorption and pulse-shaping ability. Quiet recently, we obtained the dual-wavelength soliton pulse in a passively mode-locked fiber laser incorporating a WS_2-based fiber taper, which implies that WS_2-assisted microfiber could become a mode-locker and an excellent highly-nonlinear device simultaneously [39]. Hence,

Optical Materials EXPRESS

the fiber laser with the TMD-based device may be a proper tool to study the generation and dynamics evolution of dip-type sidebands.

Here, we experimentally demonstrated the direct generation of dip-type sidebands from a passively mode-locked fiber laser by using a microfiber-based WS_2 device as both a mode-locker for soliton generation and an artificial polarizer for dip-type sidebands formation. By utilizing the saturable absorption and polarizing effect of the WS_2-deposited microfiber device, apart from the conventional Kelly sidebands, six dip-sidebands patterns, namely, dip-dip type, hybrid peak-dip and dip type (I, II), dual-peak-dip type (I, II), and nearly-flat-top type are obtained by properly adjusting the pump strength and the polarization state in the cavity. Furthermore, we found that the dynamic evolution of the dip-type sidebands along with the pump power is not reversible. Finally, we obtained the maximum depth of ~16.8 dB and ~22 dB for dual-peak-dip type I and dual-peak-dip type II, respectively, and their second-order forms. This work provides an example of the TMD-deposited microfiber device could not only be as both a mode-locker for soliton formation and but also an excellent polarizer for novel nonlinear phenomenon generation.

2. Preparation, characterization and optical properties of microfiber-based WS_2 device

The high-quality WS_2 nanosheets as-used in this experiment were prepared through the liquid-phase exfoliation method [32]. Initially, the solvent for dispersing WS_2 flakes is fabricated by mixing ethanol and water at the volume ratio of 30:70. The dispersions are treated for 2 hours by a high-power ultrasonic cleaner and settled for 10 hours. To remove large agglomeration, the WS_2 dispersion is centrifuged at 5000 rpm for 1 hour and its upper supernatant is collected. The concentration of WS_2 nanosheets in the solvent is about 0.1 mg/ml, as shown in Fig. 1(a). We transfer the WS_2 solution onto a sheet of quartz glass and dry at the room temperature so as to character its property. Then, the crystalline structure of the WS_2 material was characterized by using Raman system at 514 nm. Figure 1(b) shows the Raman spectrum of the WS_2 nanosheets in the range of 330–450 cm^{-1}. It can be clearly seen that there are two typical Raman peaks located at ~352.6 cm^{-1}, and ~418.1 cm^{-1}, which corresponds to in-plane vibrational mode E^1_{2g} and out-plane vibrational mode A_{1g} of S-W-S lattice vibration,

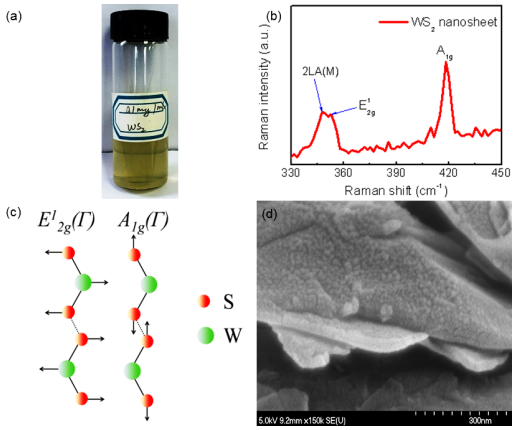

Fig. 1. Typical characteristics of the WS_2 nanosheets: (a) the WS_2 solution sample with the concentration of 0.1mg/ml, (b) the Raman spectrum of WS_2 nanosheet, (c) the diagram of vibrational energy level structure, and (d) the SEM of WS_2 nanosheets.

Optical Materials EXPRESS

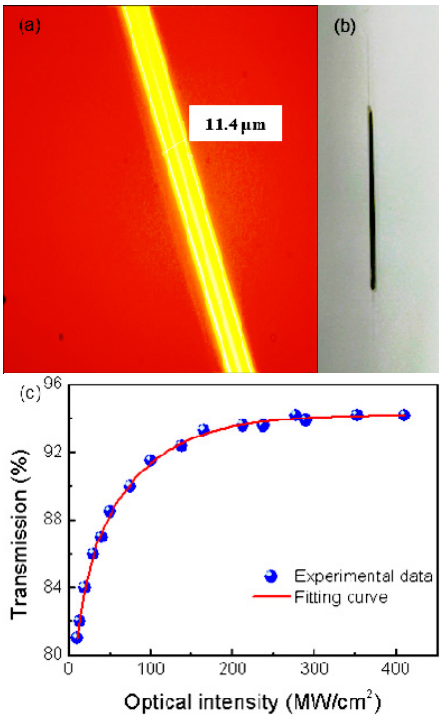

Fig. 2. (a) The photograph of the as-used microfiber, (b) the packaged microfiber-based WS_2 device, and (c) the corresponding nonlinear saturable absorption curve.

respectively, as shown in Fig. 1(c). In addition, it can be seen from Fig. 1(d), the nanosheets exhibit layer-like structure with the average thickness of ~25 nm, which implies that the layer number of WS_2 as-used is about 80 due to its single-layer thickness is about 0.315 nm [19,20].

The microfiber with the waist diameter of 11.4 μm, as shown in Fig. 2(a), was prepared by fused taper method, as reported in our previous work [39]. Then, the WS_2 nanosheets were transferred onto the waist of microfiber by using the optical deposition method, as reported in the previous work [25, 29, 30]. In order to carry out the experiment smoothly, we packaged the microfiber-based WS_2 device by using a heat shrinkable tube, as shown in Fig. 2(b). Seen clearly from the Fig. 2(c), the WS_2 device exhibits saturable absorption property and its saturation intensity and modulation depth is about 160 MW/cm^2 and 12.7%, respectively, which measured by power-dependent transmission scheme at 1550 nm. The as-used pump source is a topological insulator-assisted mode-locked fiber laser with pulse width of 500 fs and repetition rate of 15 MHz. Finally, we provided the total cavity loss of the microfiber-based WS_2 device, that is about 5 dB, which was measured with an optical power meter.

3. Experimental setup

The experimental scheme of the soliton mode-locked fiber laser is shown in Fig. 3. The pump source is a fiber-pigtailed 980 nm laser diode (980-500-B-FA, LD) and transferred the energy to a piece of ~5 m Erbium-doped fiber (Core active L-900, EDF) with dispersion parameter of ~-16.3 ps /(km· nm) via a 980/1550 wavelength-division multiplexer (WDM). The length of single mode fiber (SMF) is about 20 m and its dispersion parameter is ~18 ps/(km· nm). A 10% optical coupler (OC) is used to extract the laser output. A polarization-independent isolator (ISO) is used for unidirectional operation of the fiber laser and a polarization controller (PC) is used to adjust the polarization state in the cavity, respectively. To enhance the polarization effect in the cavity, the microfiber-based WS_2 device was spliced right after the PC. The optical spectrum, pulse information and laser power obtained is measured by an

Optical Materials EXPRESS

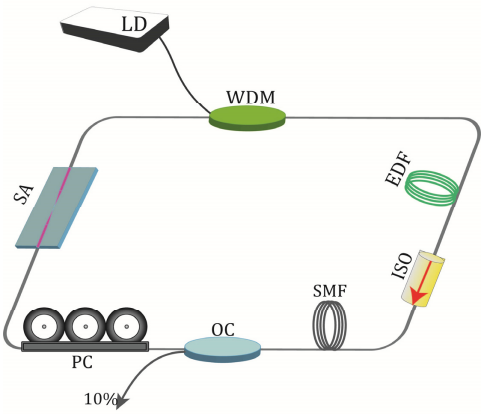

Fig. 3. Experimental setup.

optical spectrum analyzer (ANDO, AQ-6370C) with the resolution of 0.01 nm, a 1 GHz mixed oscilloscope (Tektronix MDO4054-6, 5 GHz/s) combined with a high-speed photo-detector (Thorlabs PDA, 10 GHz) and an optical power meter, respectively.

4. Results and discussions

Before carrying out the experiment, we repeatedly studied the output characteristics of the fiber laser where no microfiber-based WS_2 device placed into the cavity. The results found that whatever adjusted the pump strength and the polarization state in a very large range, there was no mode-locking appearance.

Next, a WS_2-deposited microfiber device was inserted into the laser cavity shown in the Fig. 2 (b). Initially, we obtained the continuous wave (cw) operation of the laser at ~25 mW. Then, passive mode-locking state appeared at ~35 mW, as shown in Fig. 4. As can be clearly seen from Fig. 4(a), a typical soliton spectrum of the laser with obvious symmetric Kelly sidebands appears, which indicates that the laser operates under mode-locking state. Its half wavelength full width (FWHM) is about 5.71 nm, which implies that the pulse width of the laser may be femtosecond level based on the soliton theory [40]. Meanwhile, we provided the pulse train of the laser, as shown in Fig. 4(b). It has a period of 102.5 ns, which matches with the cavity roundtrip time and indicates the fundamental repetition-rate of the fiber laser is ~9.76 MHz.

Interestingly, besides the conventional Kelly sidebands, six kinds of dip-type sideband could also be generated from the soliton mode-locked fiber laser by carefully adjusting the pump strength and polarization state in the cavity.

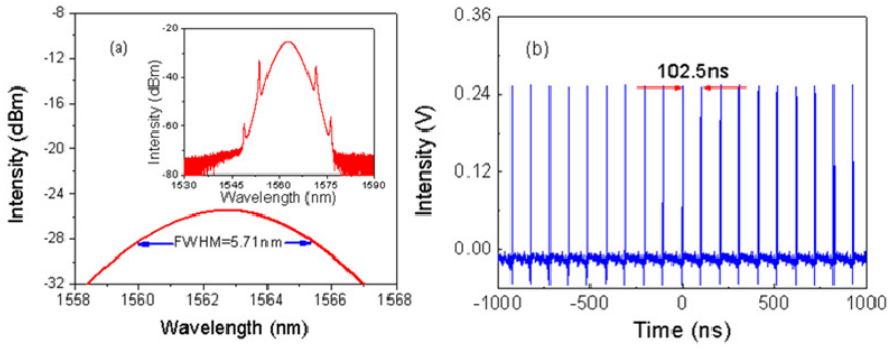

Fig. 4. Typical mode-locking pulse characteristics at the pump power of 50 mW: (a) the output optical spectrum; (b) the corresponding pulse train.

Optical Materials EXPRESS

4.1 Generation of various types of dip-type sideband

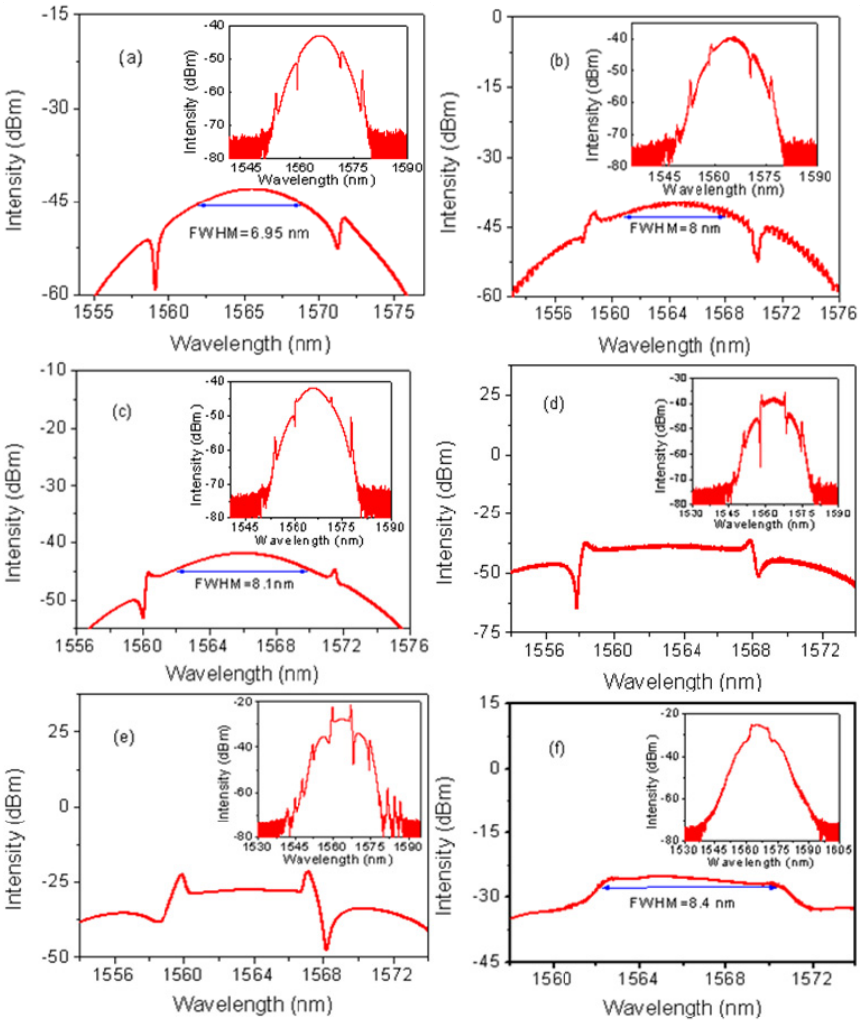

Fig. 5. Various kinds of optical spectra of the dip-type sidebands emitting from the mode-locked fiber laser with microfiber-based WS_2 device.

In experiment, there are six kinds of dip sidebands measured, namely, dip-dip type, hybrid peak-dip and dip type (I, II), dual-peak-dip type (I, II), and nearly flat-top type, as shown in Fig. 5. As the pump power increased to 60 mW, the dip-dip type sideband could be achieved by properly adjusting the orientations of PC. Figure 5(a) shows the soliton spectrum of the laser with the FWHM of 6.95 nm. It can be seen that, besides a pair of Kelly sidebands, two dips located symmetrically on the both sides of the center wavelength, which similar to that of previous report [17]. Next, let us increase the pump power to 120 mW, the dip-dip type sideband evolved dramatically into hybrid peak-dip and dip type sideband (I) shown in Fig. 5(b). Interestingly, besides Kelly sidebands, there is a peak-dip sideband and a dip sidebandlocated on the soliton spectrum, which is different from that of previous reports. By properly rotating the PCs, we can also obtain the hybrid peak-dip and dip-type sideband (II), as shown in Fig. 5(c). Then, we increased the pump power to 310 mW and rotated the PCs, a pair of peak-dip sidebands located on the soliton spectrum shown in Fig. 5(d). In this case, besides four pair of Kelly sidebands, a pair of peak-dip sidebands will be located symmetrically on the optical spectrum of the mode-locked pulses. Because the depth of right-

Optical Materials EXPRESS

dip sideband is larger than that of left-dip sideband, we call it dual-peak-dip type sideband (I), which is just opposed to the case of the dual-peak-dip type sideband (II), as shown in Fig. 5(e). Finally, let us continually increase the pump power to ~330 mW, the peak spectral sideband and dip-type sideband suddenly disappear. In this case, we call it nearly flat-top-type sideband, as shown in Fig. 5(f). Notably, this nearly-flat-top-type sideband with the FWHM of 8.4 nm can be kept stably until the pump power reaches to 420 mW.

In this experiment, we also found that the dynamic evolution of the dip-type sideband along with the pump power was not reversible, as shown in Fig. 6 and Fig. 7. In other words, the spectral sidebands exhibit different physical characteristics as the pump power increasing and the decreasing. In the next section, we would present the dynamic evolution of the mode-locked pulses with dip-type sideband in the two cases of the pump power increasing and decreasing, respectively.

As the pump power gradually increases, the optical spectra of soliton pulses with dip-type sidebands evolve as follows. 1) The laser can reach the soliton mode-locking state with clear dip-type sideband when the pump power gradually reaches to 60 mW, as shown in Fig. 6(a). Hence, the generation of the dip-type sidebands is a threshold effect which appears only if the soliton intensity is greater than a certain threshold value. It can be seen that, there are several pair of Kelly sidebands located symmetrically on the soliton spectrum which implies that the fiber laser enters in the mode-locking state. Interestingly, yt can be seen that, at the long wavelength side, the Kelly sidebands show more number and larger intensity. This is because, according to the soliton theory [40], when the laser cavity dispersion is negative, the third-order dispersion mainly takes effect on the leading edge of the soliton spectrum, thus, oscillation of low-frequency side becomes stronger in the whole spectrum. Notably, besides the Kelly sidebands, two pair of dip-type sidebands appeared on the optical spectrum and symmetric with respect to the central wavelength: the first one with the depth of ~7.5 dB and ~5 dB at 1561.9 nm and 1572.2 nm, respectively, the second one with the depth of 0.2 dB at 1557.8 nm and 1575.2 nm. In addition, a strong cw spike (~20 dB) appears near1564.75nm, which can be caused by the incomplete mode-locking under relatively weak pump strength. 2) The fiber laser would reach to new soliton mode-locking state with dip-type sidebands as the pump power gradually reaches to 310 mW shown in Fig. 6(b). Different from Fig. 6(a), at long wavelength side, the number of the Kelly sidebands decreases but their intensity still increases. This is because, as the pump power increases, nonlinear effect significantly enhances and offset the part of third-order dispersion, thus weakens the role of the third-order dispersion. Once again, a pair of dip-type sidebands with the depth of ~10 dB and ~3 dB located at 1561.3 nm and 1572 nm, respectively. Naturaly, there was a diminished cw spike (~10 dB) at 1564.7 nm. 3) The laser remains the soliton mode-locking state with dip-type sideband as the pump power gradually reaches to 320 mW shown in Fig. 6(c). Compare to the Fig. 6(b), at the long wavelength side, the number of the Kelly sidebands can be seen clearly and their intensity increases. Here, a pair of dip-type sideband with the depth of ~10 dB and ~3 dB located at 1560.9 nm and 1571.8 nm, respectively. Notably, there is no cw spike exists on the whole optical spectrum. It should note that, there is only a dip-peak sideband with the depth of ~6 dB at 1582 nm, its formation needs further exploration in section 4.2. 4) The laser evolves into another soliton mode-locking state with dip-type sideband as the pump power reaches to 330 mW, as shown in Fig. 6(d). Different from the Fig. 6(c), in the whole spectrum, the Kelly sidebands almost disappear, especially at the long wavelength side, and their intensity significantly weakens, which means that the role of the cavity nonlinearity has been dominant. In addition, a pair of dip-type sidebands with the same depth of ~1 dB still located at1561.5 nm and 1572.3 nm, respectively. After that, the shape of the spectrum remains unchanged as the pump power is eventually reach to 420 mW.

In experiment, we also found that the optical spectra of soliton pulses with dip-type sideband shows different characteristics as the pump power gradually decreases. 1) The laser operates still in the soliton mode-locking state with clear dip-type sideband when the pump power reaches to 420 mW shown in Fig. 7(a). Similar to the Fig. 6(d), a pair of dip-type sidebands

Optical Materials EXPRESS

with the same depth of ~1 dB located at 1561.4 nm and 1572.2 nm, respectively. 2) The laser enters into new soliton mode-locking state with dip-type sidebands when the pump power gradually reaches to 180 mW as shown in Fig. 7(b). Similar to the Fig. 6(c), a pair of dip-type sidebands with the depth of ~10 dB and ~3 dB located at 1560.6 nm and 1571.6 nm, respectively. Clearly, there was also a diminished cw spike (~10 dB) at 1564.7 nm. 3) The laser enters the new mode-locking state with dip-type sidebands as the pump power gradually reaches to 120 mW illustrated in Fig. 7(c). Notably, compared to the Fig. 6(b), there is only a pair of dip-type sidebands with the weakening of the depth of ~4 dB and ~2 dB located at 1559.8 nm and 1571.8 nm, respectively. 4) The fiber laser evolves into another soliton mode-locking state with dip-type sideband as the pump power continually decreases from 120 mW to 50 mW shown in Fig. 7(d). Here, there is only a pair of dip-type sidebands with the same depth of ~8 dB located at 1559.4 nm and 1572 nm, respectively. Thereafter, the laser enters into cw state as the pump power continually reduced.

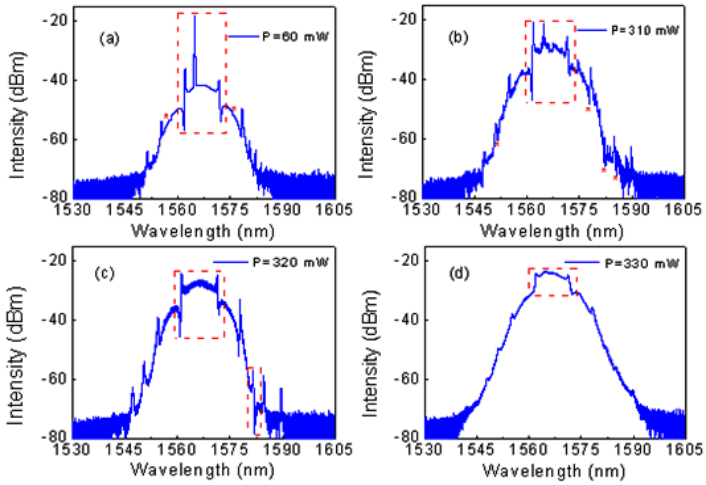

Fig. 6. The optical spectrum evolution of the dip-sideband soliton with the pump power increasing, Red dashed box marks the top of dip-type sideband spectra. '*' marks dip sideband.

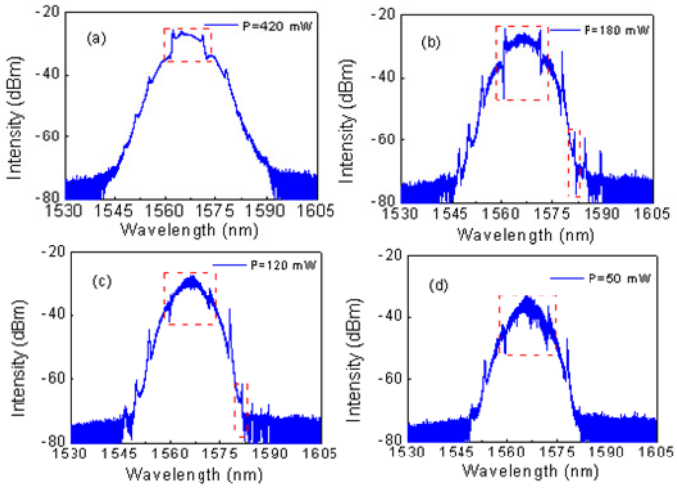

Fig. 7. The optical spectrum evolution of the dip-sideband soliton with the pump power decreasing, Red dashed box marks the top of dip-type sideband spectra and their second-order forms.

Optical Materials EXPRESS

4.2 The depth of dip-type sidebands and its second-order form

To further reveal the physical nature of the dip-type sidebands, we focus our discussion on its depth evolution and second-order form as follows. By carefully adjusting the PC, the depth of dip-type sideband would gradually increase with the pump power increasing shown in Fig. 8. In experiment, we achieved the maximum depth of ~16.8 dB and ~22 dB for dual-peak-dip type I and dual-peak-dip type II, as illustrated in Fig. 8, respectively. The study found that the generation of the dip-type sidebands is attributed to the effect of four-wave mixing between the soliton and dispersive wave which caused by the strong periodic energy exchange in the fiber laser [17]. Thus, if the laser energy flows from the soliton to the dispersive wave, a dip-sideband would be generated from the fiber laser.

Furthermore, we also obtained the second-order form of dual-peak-dip type I by properly adjusting the PC and pump power shown in Fig. 9. We noticed that the high-order form of dual-peak-dip type I always appeared at the long-wavelength side. As mentioned in 4.1, according to the soliton theory [40], when the laser cavity dispersion is negative, the high-order dispersion mainly takes effect on the leading-edge of the soliton spectrum, thus, the oscillation of the long-wavelength side becomes stronger in the spectrum. We believe that, if the pump power is bigger, there will be more high-order form can be found in the future work.

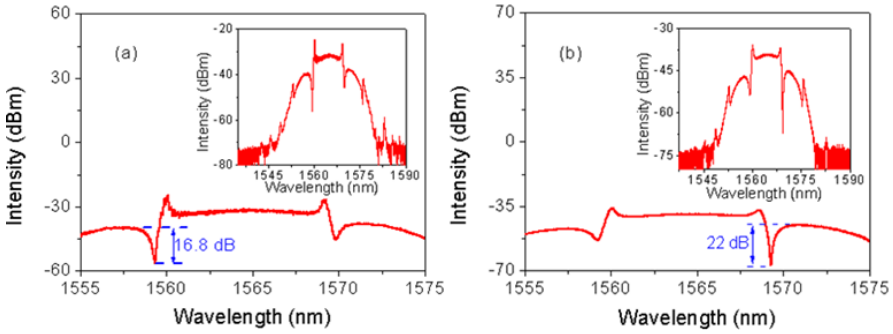

Fig. 8. The depth of the hybrid peak-dip and dip-type sideband (I) and (II).

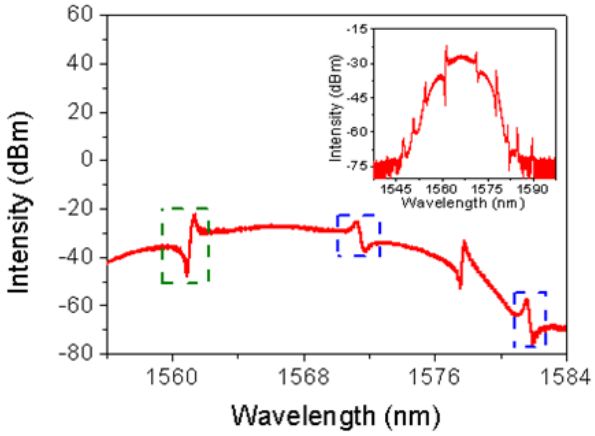

Fig. 9. The second-order form of the dual-peak-dip type (I), Green dashed box marks the left dip-peak sideband, blue dashed box marks the right dip-peak sideband and its second-order form.

4.3 The formation mechanism of dip-type sidebands

To understand the formation mechanism of the dip-type sidebands in our laser cavity, we noticed that dip-type sidebands always appeared along with the vector solitons generation in

Optical Materials EXPRESS

the fiber lasers based on many mode-locked schemes, such as SESAM [41], carbon nanotubes [42], graphene [43], and NALM [44]. It is found that, vector soliton can be generated in the fiber lasers through polarization effect or cross phase modulation when one or more optical fields are launched into the cavity, respectively. For the former, it needs the coupling between two orthogonally polarized components of a single optical field and can be achieved by a single circle cavity. For the latter, it usually needs the coupling between the two or more different optical fields and can be achieved by the two-cavity laser, such as NALM scheme. As mentioned above, several groups have indirectly observed the dip-type sidebands by inserting a polarizer outside the cavity to resolve the orthogonally polarized components [41–43]. Furthermore, they found that the dip-type sidebands always appeared in the vertical axis of polarized components, which corresponds to the s-polarization [43]. To observe the dip-type sidebands directly, Zhao *et al.* proposed a soliton mode-locked fiber laser by exploiting the NPR, which consists of two PCs and a polarization-dependent isolator [17]. However, it is surprised that stable dip-type sidebands still generate in our fiber laser even no polarizer exists. The reason is simply explained as follows.

So far, there are four common polarizers exist, namely, sheet polarizer operated by anisotropic absorption media, prism polarizer operated by refraction, Brewster-angle polarizer operated by reflection [45], and in-line fiber polarizer which relies on polarization-selective coupling between the evanescent field and birefringent crystal [46] or metal [47]. Compared with conventional polarizers, the in-line fiber polarizer is easily compatibility with most fibre-optic systems. In 2011, Bao *et al.* demonstrated a broadband graphene-based fiber polarizer by utilizing the interaction of evanescent field between side-polished fiber and graphene [48]. They found that the polarizer exhibits a strong s-polarization effect. Besides side-polished fiber, Luo *et al.* also fabricated a graphene polarizer by optically depositing graphene onto the microfiber [49]. Through these works, we found that the formation of the polarization-selective property of the fiber polarizer is related to the evanescent field interaction of optical field with graphene.

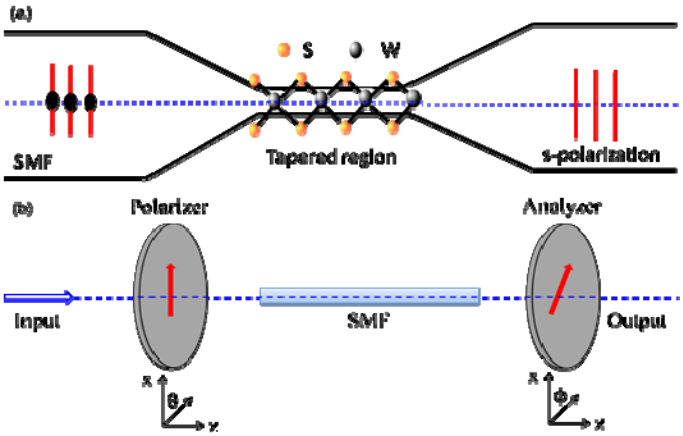

Fig. 10. (a) Polarization-selective scheme of microfiber-based WS_2 device, and (b) An equivalent setup in the cavity, which is similar to NPR mechanism, polarization angle θ and φ is defined as the angle between the polarization direction of the analyzer and the WS_2 plane.

Interestingly, similar to graphene, we also revealed that WS_2 nanosheet itself shows huge third-order nonlinearity and facilitates the multi-wavelength soliton pulse generation [39]. In this experiment, we fabricated a microfiber and optically deposited the few-layer WS_2 onto it, the structure of tapered fiber and WS_2 nanosheet itself will enhance the evanescent field interaction of optical field with WS_2 together. In the deposition process, the wide distribution of WS_2 nanosheets on the microfiber may also leads to the asymmetric absorption of the WS_2 device. Therefore, we can expect that, if WS_2 nanosheets were optically transferred onto a microfiber, the device will exhibit a strong polarization effect and form an artificial in-line

Optical Materials EXPRESS

fiber polarizer. By taking advantage of the WS_2 fiber polarizer, we obtained several kinds of dip-type sideband and their high-order forms, which was obviously different from the previous reports [41–44]. It should note that, compared with the effect of shrinkable tube, the microfiber-based WS_2 device should play a more important role for the generation of dip-type sidebands. Furthermore, to verify whether the dip-type sidebands caused by the microfiber-based WS_2 device, we tested the operation characteristic of the fiber laser without incorporating it in the cavity. By adjusting the pump strength and the cavity polarization state in a wide range, there is no mode-locking generation. Thus, this microfiber-based WS_2 device may act as a polarizer and a mode-locker in the cavity simultaneously, which facilitates the direct generation of the dip-type sidebands.

Finally, two points should be noted: 1) According to the previous works [48, 49], the polarization-selective property of the WS_2 fiber polarizer is similar to the graphene-based TE polarizer, as shown in the Fig. 10(a). This can be attributed to their the same level of high nonlinearity and similar tapered structure. 2) Since the microfiber-based WS_2 device can be viewed as a virtual polarizer, the whole setup in the cavity is equivalent to the NPR, as shown in the Fig. 10(b). Then, a question will be arised naturally: what is the mode-locking mechanism in the cavity? We believe that, WS_2 SA should play an important role for the soliton pulse generation according to its saturable absorption property, shown in Fig. 2(c). In addition, further investigation with full theoretical analysis on whether the NPR mechanism or hybrid mode-locking exists is still required in future work.

5. Conclusion

We experimentally achieved the direct generation of dip-type sidebands from a soliton mode-locked fiber laser incorporating with a microfiber-based WS_2 device. The WS_2-deposited microfiber could both operate as a mode-locker for soliton generation and induce a strong polarization effect to constitute an artificial polarizer for dip-type sidebands formation. By utilizing the saturable absorption and polarizing effect of the WS_2-deposited microfiber, six kinds of dip-sidebands, that is, dip-dip type, hybrid peak-dip and dip type (I, II), dual-peak-dip type (I, II), and nearly flat-top type was obtained by carefully adjusting the pump power and the polarization state in the cavity. In experiment, we found that the dynamic evolution of the dip-type sideband along with the pump power is not reversible. Furthermore, we also achieved the maximum depth of ~16.8 dB and ~22 dB for dual-peak-dip type I and dual-peak-dip type II, respectively, and their second-order forms. Our study indicates that the microfiber-based WS_2 device could be as an excellent optoelectronic device for studying a great deal of nonlinear phenomena.

Acknowledgments

This work was financially supported by the National Natural Science Foundation of China under Grant 61575050 and Grant 61505039, the 111 project (B13015) of the Harbin Engineering University, and China Postdoctoral Science Foundation (2015M581446).